# Multimodal layer modeling reveals *in-vivo* pathology in ALS

Alicia Northall[1,6], Juliane Doehler[1,6], Miriam Weber[2], Igor Tellez[1], Susanne Petri[3], Johannes Prudlo[4,5], Stefan Vielhaber[2], Stefanie Schreiber[2,6,7,†] and Esther Kuehn[1,7,8,9,†]

[†]**These authors contributed equally to this work.**

## Abstract

Amyotrophic lateral sclerosis (ALS) is a rapidly progressing neurodegenerative disease characterised by the loss of motor control. Current understanding of ALS pathology is largely based on the *post-mortem* investigation of advanced disease. A precise *in-vivo* description of the microstructural changes that characterize early disease stages, and their subsequent development, is therefore lacking.

Recent advances in ultra-high field (7T) MRI modelling allow us to investigate microcircuits, such as cortical layers, *in-vivo*. These automated methods reveal microarchitectural changes in the sub-millimeter range. To apply these methods of *in-vivo* histology to living ALS-patients, we used sub-millimeter qT1 and QSM data with functional localizers of cortical fields. We precisely characterized the *in-vivo* pathology in the primary motor cortex (M1) in 12 ALS-patients, in reference to 12 age-, gender-, education- and handedness-matched controls. Longitudinal sampling was performed for a subset of patients. We calculated multimodal pathology maps separately for the superficial layers (layers 2-3), layer 5a, layer 5b and layer 6 of M1 to identify hotspots of demyelination, iron and calcium accumulation in M1, both in behaviorally affected and non-affected cortical fields.

Multimodal *in-vivo* pathology maps reveal critical insights into ALS disease mechanisms. We show that despite layer-specific substance accumulation, the principal layer architecture of M1 is preserved in early disease stages. We identify multiple, small hotspots of pathology within, but also beyond, the first-affected cortical field. In addition, we localize iron accumulation to layer 6, and calcium accumulation to the superficial layer and layer 5a. Longitudinal data show that hotspots of non-topographic calcium accumulation tend to precede demyelination at later time points, where the middle-superficial layers are most

affected. These microstructural changes were in accordance with the loss of motor control, as assessed using quantitative behavioral markers of motor function.

We show that layer-specific markers of *in-vivo* pathology can be identified in ALS-patients with a single 7T-MRI measurement after first diagnosis, and that such data provide critical insights into the individual disease state. Our data highlight the non-topographic architecture of ALS disease spread, and the role of calcium rather than iron accumulation in predicting future demyelination. We also highlight a potentially important role of low-myelin borders, that are known to connect to multiple areas within the M1 architecture, in disease spread. Our findings highlight the importance of *in-vivo* histology for the diagnosis and prognosis of neurodegenerative diseases.

**Author affiliations:**

1 Institute for Cognitive Neurology and Dementia Research (IKND), Otto-von-Guericke University Magdeburg, Magdeburg, 39120, Germany

2 Department of Neurology, Otto-von-Guericke University Magdeburg (OVGU), Magdeburg, 39120, Germany

3 Department of Neurology, Hannover Medical School (MHH), Hanover, 30625, Germany

4 Department of Neurology, Rostock University Medical Centre, Rostock, 18147, Germany

5 German Center for Neurodegenerative Diseases (DZNE), Rostock, 18147, Germany

6 German Center for Neurodegenerative Diseases (DZNE), Magdeburg, 39120, Germany

7 Center for Behavioral Brain Sciences (CBBS) Magdeburg, Magdeburg, 39120, Germany

8 German Center for Neurodegenerative Diseases (DZNE), Tübingen, 72076, Germany

9 Hertie Institute for Clinical Brain Research (HIH), Tübingen, 72076, Germany

Correspondence to: Alicia Northall

Institute for Cognitive Neurology and Dementia Research (IKND)

Otto-von-Guericke University Magdeburg

Magdeburg, 39120

Saxony-Anhalt, Germany

alicia.northall@med.ovgu.de

alicia.northall@well.ox.ac.uk

**Running title**: In-vivo pathology in ALS

**Keywords:** biomarker; neurodegeneration; individualized medicine; disease prediction; motor neuron disease

**Abbreviations:** ALS = amyotrophic lateral sclerosis; ALSFRS-R = ALS Functional Rating Scale - Revised; LMN = lower motor neuron; UMN = upper motor neuron; PUMNS = Penn upper motor neuron scale; CNS-LS = Center for Neurologic Study - Lability Scale; CNS-BFS = Center for Neurologic Study - Bulbar Function Scale; DPR = disease progression rate; MP2RAGE = Magnetisation Prepared 2 Rapid Gradient Echoes; SWI = susceptibility weighted imaging; QSM = quantitative susceptibility mapping; pQSM = positive QSM; nQSM = negative QSM; qT1 = quantitative T1; M1 = primary motor cortex; 6MWT = 6-Minute-Walk-Test; TT = tongue tracker.

# Introduction

Amyotrophic lateral sclerosis (ALS) is a rapidly progressing neurodegenerative disease resulting in the loss of motor control with a median survival time of 3 years[1,2]. It affects both upper (UMN) and lower (LMN) motor neurons[1], where symptoms initially present focally in one limb or in the bulbar muscles. The disease spreads topographically, often first to the contralateral limb[3], eventually resulting in bulbar symptoms which are associated with poorer outcomes[4]. Current knowledge of ALS pathology is largely based on *post-mortem* evidence[5-7], therefore reflecting advanced disease stages. A detailed understanding of early-stage ALS pathology, in addition to mechanisms of disease spread, is needed to facilitate earlier diagnosis and improve stratification in clinical trials. Such advances may identify novel therapeutic targets to slow disease progression.

*Post-mortem* ALS studies have revealed abnormalities in the primary motor cortex (M1), where the UMNs originate, such as the depopulation of Betz cells in cortical layer 5(b)[5], iron accumulation in deep cortex[6] and increased intracellular calcium[7]. Since standard MRI cannot detect these layer-specific features, our understanding of *in-vivo* ALS pathology is limited. Disease mechanisms are therefore still debated, such as the focal hit versus multifocal pathology hypotheses[8]. Recent advances in ultra-high field MRI enable the automated assessment of anatomically-relevant cortical layers *in-vivo*[9-11], allowing us to achieve *in-vivo* histology. The present study aims to employ this approach to provide a systematic description of *in-vivo* M1 pathology in early-stage ALS.

Previous MRI studies have provided evidence for iron accumulation in M1 of ALS-patients[12-14]. The has been approximately localized to deep M1, where it corresponds to neuroinflammation and microglia activation[6,15], in addition to UMN impairment[16]. Moreover, iron accumulation affects the topographic area corresponding to the symptom onset site (i.e., first-affected)[17-19]. We previously showed that the topographic areas of M1 are microstructurally-distinct and should therefore be considered cortical fields[10], emphasising the need for precise localisation. Moreover, we highlighted that the lower-limb (LL), upper-limb (UL) and face (F) fields show differing levels of age-related iron accumulation[10], highlighting the importance of using age-matched controls. Calcium is also dysregulated in ALS, where increased calcium is associated with glutamate excitotoxicity and motor neuron death in animal models[20-21]. This excitotoxicity may reflect the increased excitability of human M1 in ALS[22]. It is currently unclear how calcium dysregulation relates to iron accumulation and demyelination in ALS.

The low-myelin borders between cortical fields in M1[23-24] have yet to be investigated in ALS. These borders show interruptions in myelination in the depths where the Betz cells are located[10,23], which are known to be affected in ALS[5], and are associated with different functional networks compared to cortical fields[26]. Since maladaptive proteins propagate along highly-myelinated neurons in neurodegeneration[25], these low-myelin borders may act as natural boundaries to limit disease spread. Alternatively, the degeneration of these borders may contribute to topographic disease spread between cortical fields[24].

The present study aimed to provide a systematic, quantitative description of *in-vivo* pathology in ALS-patients. We used topographic layer imaging[24] to characterize pathology with respect to both cortical layers and fields[10]. Sub-millimeter qT1 and QSM data, along with functional

localisers, were collected from 12 ALS-patients and 12 matched controls. We used increased positive QSM (pQSM) values as a marker of iron[6,15], increased qT1 values as a marker of (de)myelination[27], and decreased (more negative) negative QSM (nQSM) as a marker of calcium[28]. We extracted microstructural profiles from each cortical layer (superficial, layer 5a, layer 5b, layer 6) according to a previously published approach[9-10], and computed multimodal *in-vivo* pathology maps. We then tested whether (i) the layer architecture of M1 is degenerated, (ii) whether iron accumulation is layer-specific, (iii) whether the accumulation of iron and calcium is topographic (i.e., largely restricted to the first-affected cortical field), (iv) whether there are single or multiple pathology hotspots, (v) whether iron and/or calcium accumulation areas precede demyelination, and finally (vi) whether the low-myelin borders are degenerated.

# Materials and methods

## Participants

12 patients with ALS (P, 6 females, age: 60.5 ± 12.7) and 12 healthy controls (C, 6 females, age: 61.1 ± 11.9) took part in the present study between June 2018 and December 2022. Controls were individually matched to patients based on age (± 2 years; $t(22) = -.15$, $p = .883$), handedness, gender and years of education (± 4 years; patients: $M = 14.5$, $SD = 2.7$; controls: $M = 15.4$, $SD = 2.7$; $t(22) = -.82$, $p = .422$). On average, patients were measured within 3 months of diagnosis ($SD = 5$, range: 0-14) and within 19 months of symptom onset ($SD = 13$, range: 2-48). Note that this excludes one patient (P4) with a very long disease duration (166 months between MRI and diagnosis). Participants underwent 7T-MRI and behavioural assessments. 3 patients (P1, P2, and P4) were measured again within 1 year (T2), while 1 patient (P4) was also measured 8 months after T2 (T3). Patients were recruited from the Otto-von-Guericke University Magdeburg, Hannover Medical School and Rostock University Medical Center (see **Table 1**). An experienced neurologist performed clinical assessments (see **Table 2**). Of the 12 patients, 7 had upper limb-onset (UL-onset; 3 right-lateralized, 2 left-lateralized, 1 bilateral), 2 had lower limb-onset (LL-onset; both left-lateralized) and 3 had bulbar-onset (B-onset; considered bilateral). Controls were recruited from the DZNE database in Magdeburg, and exclusion criteria included sensorimotor deficits, neurologic disorders and 7T-MRI contraindications. Participants gave

written informed consent and were paid. The study was approved by the local Ethics Committee of the Medical Faculty of the University of Magdeburg.

| Patient | Age (years) | Education (years) | Gender | Handedness | Onset type | Onset side | Phenotype | El-Escorial | MRI-Symptoms (months) | MRI-Diagnosis (months) |
|---|---|---|---|---|---|---|---|---|---|---|
| P1 | 50 | 13 | F | R | UL | L | LMND | Possible | 12 | 5 |
| P2 | 66 | 18 | M | R | UL | L | UMND | Probable | 12 | 0 |
| P3 | 60 | 12 | M | L | UL | L | UMND | Definite | 12 | 0 |
| P4 | 48 | 13 | M | R | UL | R | Classical | Definite | 189 | 166 |
| P5 | 77 | 14 | F | R | UL | R | LMND | Definite | 29 | 14 |
| P6 | 73 | 15 | M | R | UL | B | Classical | Definite | 14 | 5 |
| P7 | 74 | 15 | F | R | LL | L | UMND | Definite | 17 | 0 |
| P8 | 36 | 16 | M | R | LL | L | Classical | Probable | 28 | 4 |
| P9 | 52 | 12 | F | R | UL | R | UMND | Possible | 48 | 0 |
| P10 | 53 | 21 | M | R | B | B | Classical | Definite | 32 | 12 |
| P11 | 64 | 13 | F | R | B | B | LMND | Possible | 7 | 0 |
| P12 | 72 | 12 | F | R | B | B | LMND | Definite | 2 | -5 |

**Table 1.** Clinical and demographic information for patients with ALS (*n* = 12). The El-Escorial criteria indicates the degree of certainty of ALS diagnosis[28]. MRI-Symptoms indicates the time in months between the MRI and symptom onset, while MRI-Diagnosis indicates the time in months between MRI and formal diagnosis. Note that a negative MRI-Diagnosis indicates that the patient was scanned prior to a formal diagnosis. Gender: F - female, M - male; Handedness: R - right, L - left; Onset type: UL - upper limb-onset type, LL - lower-limb onset type, B - bulbar-onset type; Onset side: L - left, R - right, B - bilateral; Phenotype: LMND - lower motor neuron dominant; UMN - upper motor neuron dominant, classical - both upper and lower motor neuron impairment.

| Patient | PUMNS | ALS-FRS-R total | ALS-FRS-R fine motor | ALS-FRS-R gross motor | ALS-FRS-R bulbar | CNS-LS | CNS-BFS | Disease Progression Rate |
|---|---|---|---|---|---|---|---|---|
| P1 | 1 | 44 | 9 | 11 | 12 | 14 | 22 | 0.24 |
| P2 | 3 | 41 | 9 | 11 | 9 | 11 | 31 | 0.64 |
| P3 | 11 | 40 | 7 | 10 | 12 | 15 | 32 | 0.73 |
| P4 | 2 | 37 | 6 | 7 | 12 | 7 | 21 | 0.06 |
| P5 | 0 | 35 | 2 | 9 | 12 | 7 | 24 | 0.48 |
| P6 | 9 | 34 | 2 | 8 | 12 | 7 | 23 | 1.00 |
| P7 | 22 | 25 | 6 | 3 | 7 | 30 | 53 | 1.77 |
| P8 | 15 | 45 | 12 | 9 | 12 | 7 | 22 | 0.12 |
| P9 | 16 | 42 | 10 | 9 | 12 | 19 | 22 | 0.13 |

| | | | | | | | | |
|---|---|---|---|---|---|---|---|---|
| P10 | 2 | 33 | 9 | 9 | 7 | 10 | 62 | 0.45 |
| P11 | 1 | 47 | 12 | 12 | 11 | 25 | 28 | 0.17 |
| P12 | 1 | 46 | 12 | 12 | 10 | 7 | 32 | 1.00 |

**Table 2.** Clinical assessment scores for patients with ALS (*n* = 12). PUMNS - Penn Upper Motor Neuron Scale; ALS-FRS-R: ALS Functional Rating Scale - Revised; CNS-LS: Center for Neurologic Study-Lability Scale; CNS-BFS: Center for Neurologic Study - Bulbar Function Scale; Disease Progression Rate: 48-(ALSFRS-R total)/MRI-Symptoms. The ALSFRS-R[29] indicates disease severity, where lower values indicate greater impairment, with subscores for fine, gross and bulbar motor function. The CNS-LS[30] indicates the frequency of pseudobulbar episodes, with higher scores indicating greater impairment. The CNS-BFS[31] indicates bulbar dysfunction, with higher scores indicating greater impairment. Finally, the PUMNS[32] score indicates the presence of pathological reflexes, with higher scores indicating greater impairment (*M* = 7, *SD* = 7, range: 0-22).

# 7T-MRI Data Acquisition

Data were collected using a 7T-MRI scanner equipped with a 32-channel head coil (MAGNETOM, Siemens Healthcare), located in Magdeburg, Germany. We acquired whole-brain, 0.7mm isotropic resolution MP2RAGE images[34] (sagittal slices, repetition time = 4800 ms, echo time = 2.01 ms, field-of view read = 224 mm, GRAPPA 2, flip angle = 5◦/3◦, inversion time TI1/TI2 = 900/2750 ms, bandwidth = 250 Hz/Px) and whole-brain, 0.5-mm isotropic resolution susceptibility-weighted (SWI) images in 10/12 patients (transversal slices, repetition time = 22 ms, echo time = 9 ms, field-of view read = 192 mm, GRAPPA 2, flip angle = 10◦, bandwidth = 160 Hz/Px), where 2 patients could not be scanned due to fatigue and discomfort. We also acquired a whole-brain, 1.5 mm isotropic resolution functional image (81 slices, repetition time = 2000 ms, echo time = 25 ms, field-of-view read = 212 mm, GRAPPA 2, interleaved acquisition) using an EPI gradient-echo BOLD sequence. The functional imaging involved a blocked-design paradigm with 12-second periods of body part movements (left/right foot, left/right hand, tongue) alternated with 15-seconds of rest (as described previously[10]). Before scanning, participants were trained in the movements and patients with difficulty in conducting single movements were particularly trained to conduct a reduced amount of movement precisely. Instructions inside the scanner (gray background, black color) asked participants to prepare (e.g., ‘prepare right foot) before performing the movement (e.g., ‘move right foot’). Each movement was repeated four times, resulting in a total of 20 trials. Participants and patients wore fingerless braces covering the hands and forearms to reduce large movements of the hands and to facilitate movements of the patients. The total scanning duration was approximately 75 minutes.

# Image Processing

## Structural Preprocessing

CBS Tools (version 3.0.8)[35] in MIPAV (version 7.3.0)[36] was used to process the structural data. Skull stripping and dura estimation were used to remove extra-cranial tissue, which was refined using ITK-SNAP (version 3.8). The TOADS algorithm[37] was used to segment the brain into different tissue types, before the CRUISE module was used to estimate the boundaries between the WM, GM and CSF[38], resulting in level set images for subject-specific cortical surfaces. The volumetric layering module[39-40] was used to divide the cortex into 21 depths, according to the equivolume approach as described previously[10]. M1 masks were manually delineated using ITK-SNAP, as described previously[10].

### Quantitative Susceptibility Mapping (QSM)

After data quality checks, the SWI data of 4 patients (and the 4 matched controls) were excluded due to severe motion and truncation artifacts, leaving 16 participants for the SWI analyses. QSMbox (version 2.0) was used to reconstruct QSM from the SWI images[41]. In line with previous studies in ALS and aging[12,42], QSM values were not normalized but raw values were used. We divided the QSM data into positive QSM (pQSM) and negative QSM (nQSM) values (as previously described[42]).

## Defining Cortical Layers

Using ParaView (version 5.8.0), we calculated mean curvature and regressed it out of qT1 values at each layer, on a subject-specific basis, as previously described[10,43]. We applied a data-driven approach to identify cortical layers in M1 from group-averaged decurved qT1 profiles[9-10] (see **Fig.1B** for details, see **Supplementary Fig.1** for right hemisphere).

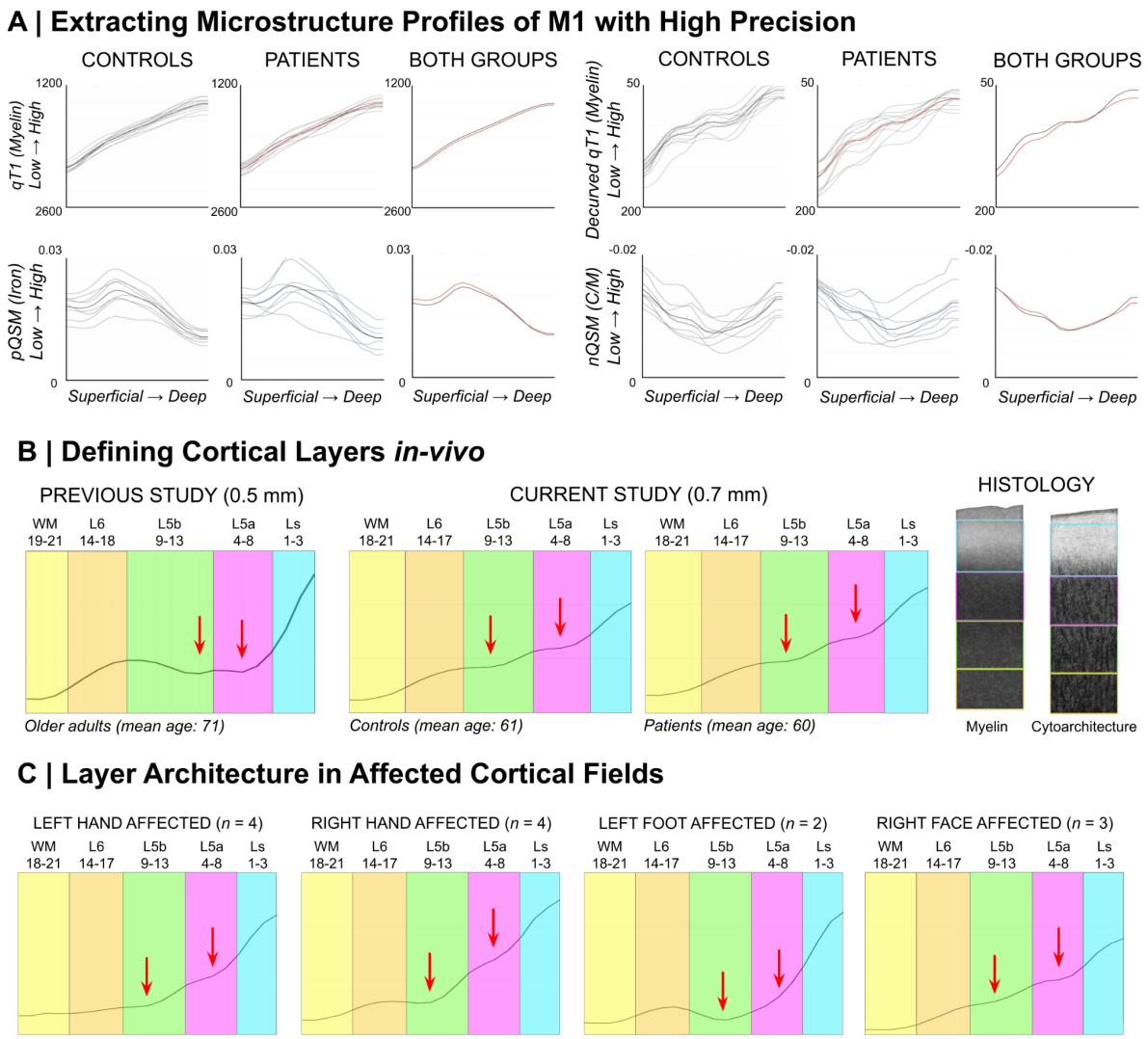


**Figure 1. Microstructure profiles of the left primary motor cortex (M1) in patients with ALS and matched controls. (A)** 'Raw qT1' (i.e. not decurved), decurved qT1, positive QSM (pQSM) and negative QSM (nQSM) data extracted across all cortical depths ($n$ = 21) of left M1. The first two columns show data for all controls and all patients, with the group mean plotted in bold black and red, respectively. The third column shows the mean group data of the controls and patients, with red lines representing the patients. Note that pQSM values represent iron, whereas nQSM values reflect calcium. Also note that the profiles here represent the data of M1, while data averaged across cortical fields was used in other figures and statistics. **(B)** According to a previously published approach[9], we identified four compartments ('layers') based on 'decurved qT1' (Ls - superficial layer including layers 3 and 4; L5a - layer 5a; L5b - layer 5b; L6 - layer 6). We show these layer definitions for healthy controls ($n$ = 12) and patients ($n$ = 12) in the present study, as well as for older adults ($n$ = 18) in our previous study[10]. L5a and L5b were distinguished based on the presence of two small qT1 dips at the plateau of 'decurved qT1' values (indicating L5), while L6 was identified based on a sharp decrease in values before a further plateau indicating the presence of white matter. We show our layer approximations over schematic depictions (*right*) of M1 myelin[55] and cell histological staining[56] are shown. **(C)** Despite differences in the shape of the profile in the affected fields compared to the average across fields in patients, layers can be similarly identified in the affected fields.

## Functional Data Processing

The functional data were preprocessed using SPM12, including realignment, slice timing and smoothing (2mm FWHM). To create the functional localisers of the cortical fields (i.e., hand,

face, and foot areas), we took the peak cluster of each t-map and removed overlapping voxels between localisers as previously described[10]. We extracted layer-wise qT1 and signed QSM values from the cortical fields, resulting in microstructural profiles for each cortical layer.

### Myelin Border Analysis

We identified myelin borders between the UL and F representations based on the highest qT1 value (i.e. lowest myelin) located between the peak t-values of the UL and F localisers, using a previously applied approach[23,44]. We extracted the qT1 values at the myelin borders and calculated the average qT1 values of the UL and F body part representations (UL+F/2).

### Layer-Specific Multimodal in-vivo Pathology Mapping

Using topographic layer imaging, we created *in-vivo* pathology maps on inflated cortical surfaces for each individual ALS-patient in reference to their matched control (see **Fig.2** and **Supplementary Fig.2**). Pathology maps were calculated to identify disease hotspots indicated by demyelination / cell loss (increased qT1, +1SD to +4SDs), iron accumulation (increased pQSM, +1SD to +4SDs) and calcium accumulation / increased metabolism (decreased nQSM, -1SD to -4SDs) in each patient, relative to the mean M1 value of the matched control. The reference values were layer-specific to control for microstructural differences between layers in M1[10]. In addition, pathology maps are shown with individually-localized cortical fields in M1, to account for microstructural differences between cortical fields[10].

## Behavioral Tests of Motor Function

All participants underwent body part-specific behavioral tests of motor function (as previously used[10]). To quantify LL function, the 6-Minute-Walking-Test (6MWT) was used to measure walking distance[45]. To quantify UL function, a dynamometer[46] was used to measure hand strength, and the Purdue[47] (Lafayette Instrument, model 32020A), Grooved[48] (Lafayette Instrument, model 32025) and O'Connor[49] (Lafayette Instrument, model 32021) pegboards were used to measure hand dexterity. To quantify bulbar (F) function, we used an automated tool that extracts features (e.g., errors, speed) of lateral tongue movements from short video clips[50].

## Statistical Analyses

Statistical analyses were performed using IBM SPSS Statistics (version 26, IBM, USA). Given the known impaired motor function in ALS-patients and the low sample size, we used one-tailed paired-samples t-tests to test for group differences. Based on evidence of demyelination, iron and calcium accumulation in ALS[5-7] and the low sample size, we used one-tailed paired-samples t-tests to test for differences in qT1, pQSM and nQSM values between groups. Note that paired-samples t-tests were used to account for dependencies in the data (i.e. matched patient-control pairs). Patient-specific pathology maps were calculated by thresholding surfaces to show demyelination (increased qT1, +1SD to +4SDs), iron accumulation (increased pQSM, +1SD to +4SDs) and calcium accumulation (decreased nQSM, -1SD to -4SDs) in each patient relative to the mean M1 value of the matched control. Pathology estimations based on 1-4 SD are often used in clinical diagnostic imaging tools as they provide a detailed overview of how much the respective pathology differs from a control brain (see e.g., AIRAscore Software). The reference values were layer-specific to control for microstructural gradients with cortical depth in M1[10].

## Data availability

The data used in the present study have been made available in a public repository (https://github.com/alicianorthall/In-vivo-Pathology-ALS).

# Results

## Impaired Motor Function in Patients with ALS

We quantified body part-specific motor function in 12 ALS-patients and 12 matched controls (LL: 6MWT; UL: hand strength, pegboards; F: tongue kinematics). For 3 patients, follow-up behaviour measurements were performed. The results show that patients with ALS are significantly impaired in motor function of all tested body parts compared to matched controls, and in most cases, the scores of the different body parts worsen over time (see **Fig.2**, see **Supplementary Table 1** for statistics).

### No Significant M1 Differences in Patients When Averaged Across Depths

We first tested if the averaged qT1 and QSM values (averaged across the (LL, UL, F) cortical fields and depths (L6, L5b, L5a, Ls) of M1 were significantly different in ALS-patients compared to controls to align with previous analyses[12,16]. Using this approach, there are no significant differences in pQSM values between patients and controls in left M1 (patients: $M$ = .0172, $SD$ = .0026; controls: $M$ = .0171, $SD$ = .0028; $t(7) = 0.2$, $p = .428$, $d = -0.037$, 95% CI [-1.02 0.94]) or right M1 (patients: $M$ = .0185, $SD$ = .0027; controls: $M$ = .0172, $SD$ = .0029; $t(7) = 1.3$, $p = .114$, $d = -0.46$, 95% CI [-1.46 0.53]). There are also no significant differences in nQSM between patients and controls in left M1 (patients: $M$ = -.0094, $SD$ = .0019; controls: $M$ = -.0085, $SD$ = .0013; $t(7) = 1.6$, $p = .081$, $d = 0.55$, 95% CI [-.45 1.55]) or right M1 (patients: $M$ = -.0089, $SD$ = .0021; controls: $M$ = -.0087, $SD$ = .0018; ($t(7) = 0.3$, $p = .375$, $d = 0.10$, 95% CI [-.88 1.08]). Finally, there are no significant differences in qT1 between patients and controls in left M1 (patients: $M$ = 1763.04 $SD$ = 82.86; controls: $M$ = 1783.64, $SD$ = 50.62; ($t(11) = 0.7$, $p = .764$, $d = .30$, 95% CI [-.54 1.14]) or right M1 (patients: $M$ = 1786.33, $SD$ = 103.15; controls: $M$ = 1816.21, $SD$ = 49.35; $t(11) = 1.0$, $p = .834$, $d = 0.37$, 95% CI [-.47 1.21]).

# Layer-Specific M1 Pathology in Patients with ALS

## M1 Layer Architecture in ALS-patients

As in our previous work[10], we used decurved qT1 values to identify four layers in M1 (Ls = superficial layer; L5a = layer 5a; L5b = layer 5b; L6 = layer 6; see **Fig.1B** for details). Our data show that those 4 layers can be identified similarly for ALS-patients and controls, where layers showed the same peaks (e.g., level set 11 for L5b) and relative thicknesses (e.g., level set 9-13 for L5b). The principle layer architecture therefore appears to be preserved in patients with early-stage ALS (see **Fig.1B**), also in the affected cortical fields (see **Fig. 1C**) although there are differences in the profile shape.

## Pathological Substance Accumulation in M1 is Layer-Specific

We extracted qT1 values as a marker of (de)myelination[27], pQSM values as a marker of iron[15], and nQSM as a proxy for calcium[28], with high precision (see **Fig.1A**). Iron accumulation is a hallmark feature of ALS pathology[6,15] and has been shown to approximately affect the deep region. We show a significant increase in pQSM, specifically

in L6 of left and right M1, in patients compared to matched controls (left M1: patients: $M$ = .0144, $SD$ = .0020; controls: $M$ = .0128, $SD$ = .0027; $t(7) = 2.0$, $p$ = .043, $d$ = 0.67, 95% CI [-0.33 1.68]; right M1: patients: $M$ = .0165, $SD$ = .0025; controls: $M$ = .0140, $SD$ = .0019; $t(7) = 2$, $p$ = .041, $d$ = 1.13, 95% CI [0.07 2.18]). We show no significant differences in pQSM between patients and controls in the other layers (L5b, L5a and Ls) of left or right M1 (see **Fig.4B**, see **Table 3** for statistics).

| | **ALS patients (n = 12)** | **Matched controls (n = 12)** | **Group difference** | | | |
|---|---|---|---|---|---|---|
| | Mean (SD) | Mean (SD) | *df* | *t* | *Sig.* | *d [95% CI]* |
| pQSM | | | | | | |
| Right L6 | .0165 (.0025) | .0140 (.0019) | 7 | 2.0 | .041* | 1.13 [.07 2.18] |
| Right L5b | .0201 (.0039) | .0191 (.0033) | 7 | 0.8 | .220 | .28 [-.71 1.26] |
| Right L5a | .0195 (.0041) | .0187 (.0039) | 7 | .07 | .253 | .20 [-.78 1.18] |
| Right Ls | .0180 (.0029) | .0170 (.0031) | 7 | 1.0 | .170 | .33 [-.65 1.32] |
| Left L6 | .0144 (.0020) | .0128 (.0027) | 7 | 2.0 | .043* | .67 [-.33 1.68] |
| Left L5b | .0184 (.0037) | .0187 (.0034) | 7 | -.40 | .360 | -.13 [-1.07 .90] |
| Left L5a | .0191 (.0030) | .0190 (.0037) | 7 | .02 | .492 | .03 [-.95 1.01] |
| Left Ls | .0170 (.0028) | .0177 (.0028) | 7 | -.60 | .727 | -.25 [-1.23 .73] |
| nQSM | | | | | | |
| Right L6 | -.0075 (.0034) | -.0074 (.0019) | 7 | .20 | .441 | .04 [-.94 1.02] |
| Right L5b | -.0064 (.0027) | -.0063 (.0015) | 7 | .20 | .443 | .05 [-.93 1.03] |
| Right L5a | -.0088 (.0021) | -.0084 (.0020) | 7 | .50 | .303 | .20 [-.79 1.18] |
| Right Ls | -.0128 (.0018) | -.0126 (.0025) | 7 | .30 | .387 | .09 [-.89 1.07] |
| Left L6 | -.0082 (.0029) | -.0076 (.0016) | 7 | .60 | .294 | .26 [-.73 1.24] |
| Left L5b | -.0069 (.0028) | -.0061 (.0014) | 7 | .90 | .210 | .36 [-.63 1.35] |
| Left L5a | -.0092 (.0019) | -.0080 (.0013) | 7 | 2.0 | .040* | .74 [-.28 1.75] |
| Left Ls | -.0134 (.0016) | -.0121 (.0014) | 7 | 2.4 | .024* | .87 [-.16 1.89] |
| qT1 | | | | | | |
| Right L6 | 1526.11 (93.37) | 1558.45 (57.37) | 11 | 1.1 | .860 | .42 [-.43 1.26] |
| Right L5b | 1676.91 (95.40) | 1708.91 (59.83) | 11 | 1.4 | .903 | .40 [-.44 1.25] |
| Right L5a | 1863.87 (110.11) | 1895.49 (52.47) | 11 | 1.0 | .826 | .37 [-.48 1.21] |

| | | | | | | |
|---|---|---|---|---|---|---|
| Right Ls | 2078.43 (132.64) | 2101.98 (40.33) | 11 | 0.6 | .706 | .24 [-.60 1.08] |
| Left L6 | 1501.84 (69.33) | 1517.70 (57.46) | 11 | 0.6 | .728 | .25 [-.59 1.09] |
| Left L5b | 1647.98 (79.63) | 1671.06 (56.68) | 11 | 0.9 | .805 | .33 [-.51 1.18] |
| Left L5a | 1863.43 (54.68) | 1841.15 (93.62) | 11 | 0.7 | .753 | -.29 [-1.13 .55] |
| Left Ls | 2061.17 (113.51) | 2082.36 (44.43) | 11 | 0.6 | .707 | .25 [-.59 1.09] |

**Table 3.** Paired group differences in layer-wise microstructure in M1 between patients (qT1: *n* = 12, QSM: *n* = 8) and matched controls (qT1: *n* = 12, QSM: *n* = 8). One tailed paired-samples t-tests were used to investigate patient-control differences in pQSM, nQSM and qT1 values in each layer. * indicates significance at the .05 uncorrected level, while no tests showed significance at the Bonferroni-corrected level (.05/32 = .002). (L6 - layer 6, L5b - layer 5b, L5a - layer 5a, Ls - superficial layer).

## Iron Accumulation in L6 of First-Affected Cortical Field

Using topographic layer imaging, we created *in-vivo* pathology maps for each individual ALS-patient in reference to matched controls (see **Fig.2**, see **Supplementary Fig.2** for patients with qT1 data only). These maps reveal that demyelination is minimal compared to iron and calcium accumulation. As expected, iron accumulation mostly occurs in the first-affected cortical field (6/8 patients, see filled red arrows in **Fig.2**), however it also occurs in unaffected body parts (non-filled red arrows in **Fig.2**). More specifically, P2, P4, P5 and P6 show iron accumulation in the UL fields, corresponding to the UL-onset type, whereas P7 and P8 show iron accumulation in the LL fields, corresponding to the LL-onset type. However, P1, P6, P7 and P8 also show iron accumulation in non-affected cortical fields, or in non-localised areas. P12 does not show iron accumulation, but shows demyelination in the F field corresponding to the B-onset type of the patient. The pathology maps also show that, in most patients, iron accumulation affects L6, which is in line with the statistical analysis.

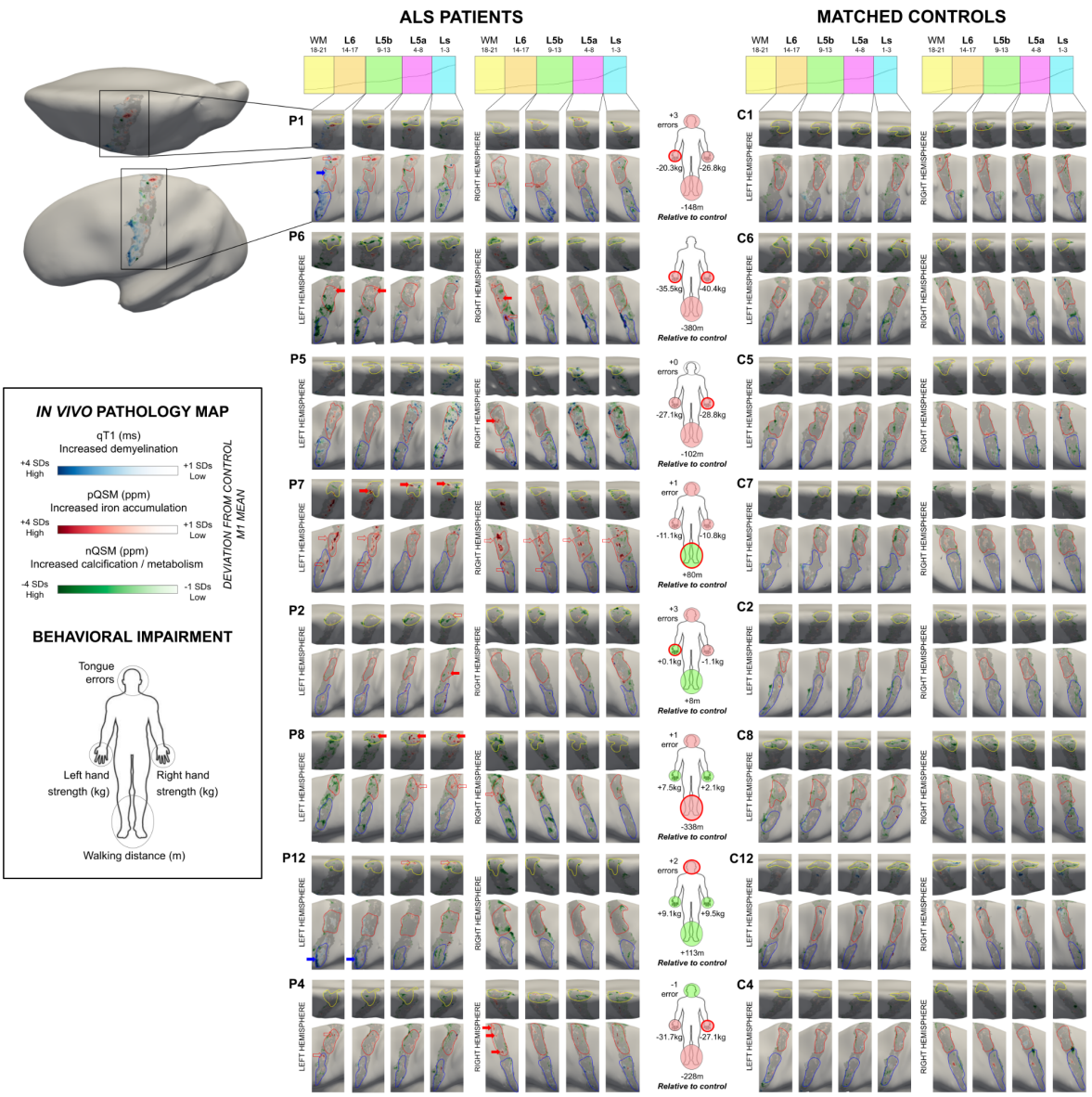


**Figure 2. Multimodal *in-vivo* pathology maps in patients with ALS.** Pathology maps were generated by thresholding the displayed value ranges at each layer to show increased qT1 and pQSM (+1 to +4 SDs), and reduced nQSM (-1 to -4 SDs), with respect to the mean M1 value of the matched control. Pathology maps are shown for P1, P2, P8, P12, P6, P7, P4 and P5 (*left*) and their corresponding matched controls C1, C2, C8, C12, C6, C7, C4 and C5 (*right*). Pathology maps: note that filled red and blue arrows indicate iron accumulation and demyelination in the first-affected cortical field, respectively. Unfilled red arrows indicate iron accumulation in cortical fields other than the first-affected field. Body maps: Note that red-outlined circles on the body maps indicate the onset site of the patient, while red and green filled circles indicate impaired or better motor function in the circled body part compared to the matched control, respectively. (L6 - layer 6, L5b - layer 5b, L5a - layer 5a, Ls - superficial layer).

## Calcium Accumulation is Non-Topographic and Encompasses Low-Myelin Borders

The pathology maps (see **Figure 2**) also provide an overview of calcium dysregulation in early-stage ALS, which show that calcium accumulation is non-topographic. The maps reveal

that in most cases (P1, P2, P5, P6, P7, P8, P12), calcification occurs in the area between major body parts, where the low-myelin borders are located. We note that P12, who did not show iron accumulation, does show calcium accumulation.

## Multiple Hotspots of Pathology in M1

We also addressed whether *in-vivo* pathology maps favour the hypothesis of one large pathology hotspot or multiple hotspots of pathology. The maps reveal that pathology occurs in multiple, small areas, often beyond the first-affected cortical field (see **Fig.2**). For example, P1 shows iron accumulation in an area between the left LL and UL fields compared to the control, while this patient shows demyelination in the (first-affected) left UL field.

## Calcium Accumulation Precedes Demyelination

Out of the 12 patients, three (P1, P2 and P4) were also measured longitudinally. Based on visual inspection, all three patients show demyelination (i.e. highly increased qT1) at measurement time point 2 (T2) compared to measurement time point 1 (T1, see **Fig.3**), and also at T2 compared to controls (see **Fig.2**). In addition, P4 showed demyelination at T3 compared to T2 (see **Fig.3**). Demyelination occurred most strongly in L5a and Ls, although P1 also showed demyelination in the deeper layers. These longitudinal pathology maps indicate that demyelination occurs at previous hotspots of calcium, rather than iron, accumulation (see **Fig.3**).

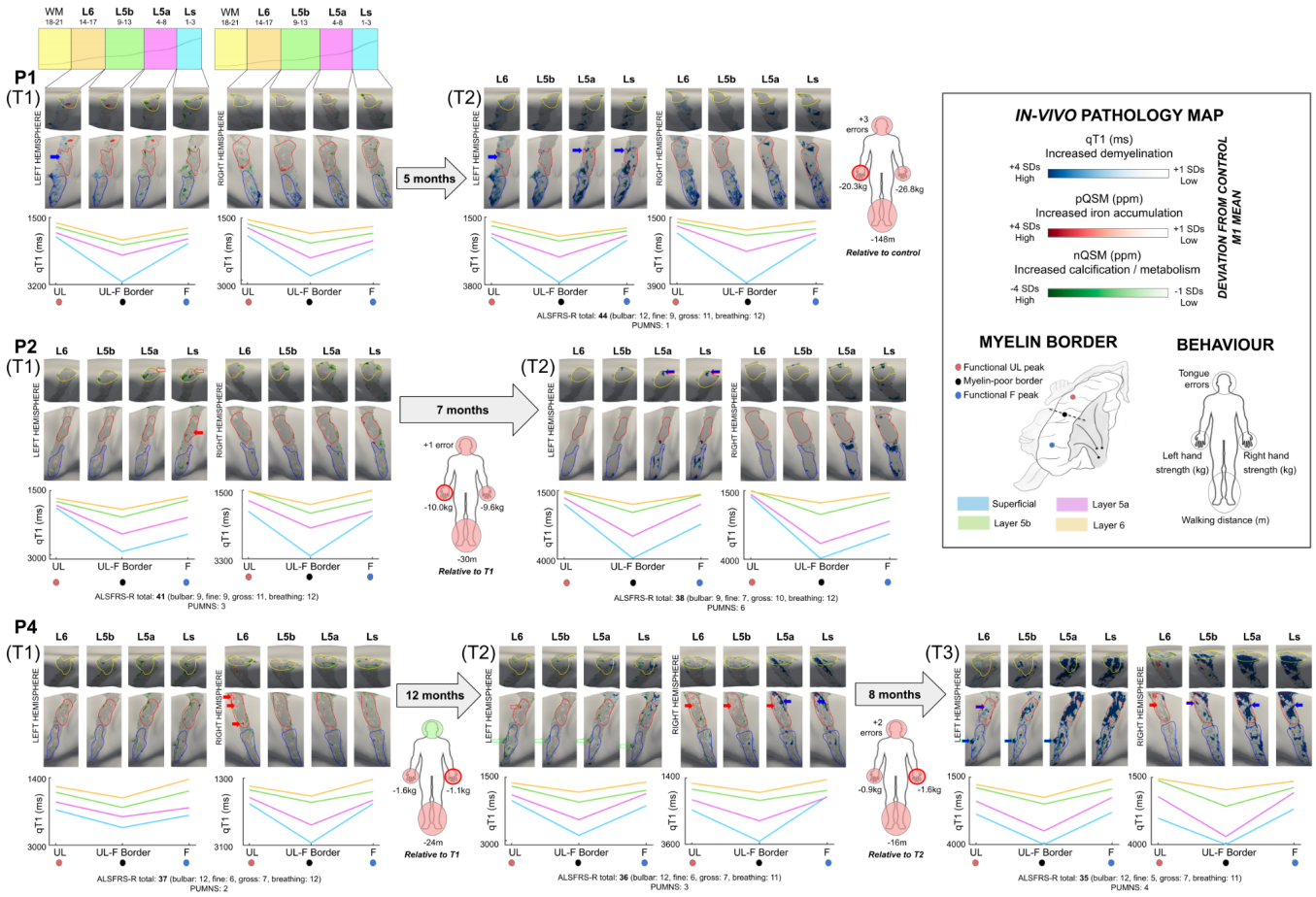


**Figure 3. Longitudinal multimodal *in-vivo* pathology maps in patients with ALS.** Individualized *in-vivo* pathology maps were generated by thresholding the displayed value ranges at each layer to show increased qT1 and pQSM (+1 to +4 SDs), and reduced nQSM (-1 to -4 SDs), with respect to the mean M1 value of the matched control at baseline. Row 1 shows the pathology maps for P1 at T1 and T2, row 2 shows the pathology maps for P2 at T1 and T2 and row 3 shows the pathology maps for P4 at T1, T2 and T3. Note that red and blue arrows on the pathology maps indicate iron accumulation and demyelination in the cortical field corresponding to symptom onset site, respectively. Note that red-outlined circles on the body maps indicate the onset site of the patient, while red and green filled circles indicate impaired or better motor function in the circled body part compared to the matched control, respectively. Note that T1, T2 and T3 indicate that data were acquired from the first, second and third time points, respectively. Note that QSM data were excluded at T2 for P1 and P2 due to severe artifacts. (L6 - layer 6, L5b - layer 5b, L5a - layer 5a, Ls - superficial layer).

### Disrupted Low-Myelin Borders With Disease Progression

We also addressed whether the low-myelin borders that separate cortical fields in M1 are perhaps particularly affected in ALS. The longitudinal pathology maps show demyelination of the hand-face border at T2 compared to T1 (see P1, P2 and P4 in **Fig.3**), and at T3 compared to T2 (see P4 in **Fig.3**). In addition, this effect is largely restricted to Ls and L5a, where the low-myelin borders are typically most defined in healthy adults[10,23]. These areas of demyelination overlap with those of calcium accumulation at T1 in the three patients.

## Discussion

ALS is a rapidly progressing neurodegenerative disease characterized by the loss of motor control[1]. The present study aimed to provide a systematic description of *in-vivo* M1 pathology in early-stage ALS-patients. Given the layer-specific nature of ALS pathology[5], we combined submillimeter structural 7T-MRI data (qT1, QSM) and automated layer modeling to achieve *in-vivo* histology. Our data reveal critical insights into ALS pathology in M1: (i) the principle layer architecture is preserved, (ii) iron accumulation is specific to layer 6, (iii) the accumulation of iron is topographic (i.e., largely in the first-affected cortical field, but also beyond), whereas calcium accumulation is non-topographic, (iv) there are multiple pathology hotspots, (v) non-topographic calcium, rather than topographic iron, precedes demyelination, and (vii) low-myelin borders between cortical fields are particularly affected with disease progression. Overall, our study provides the first systematic description of *in-vivo* pathology in ALS, offering new insights into disease mechanisms in ALS (see **Fig.4A**).

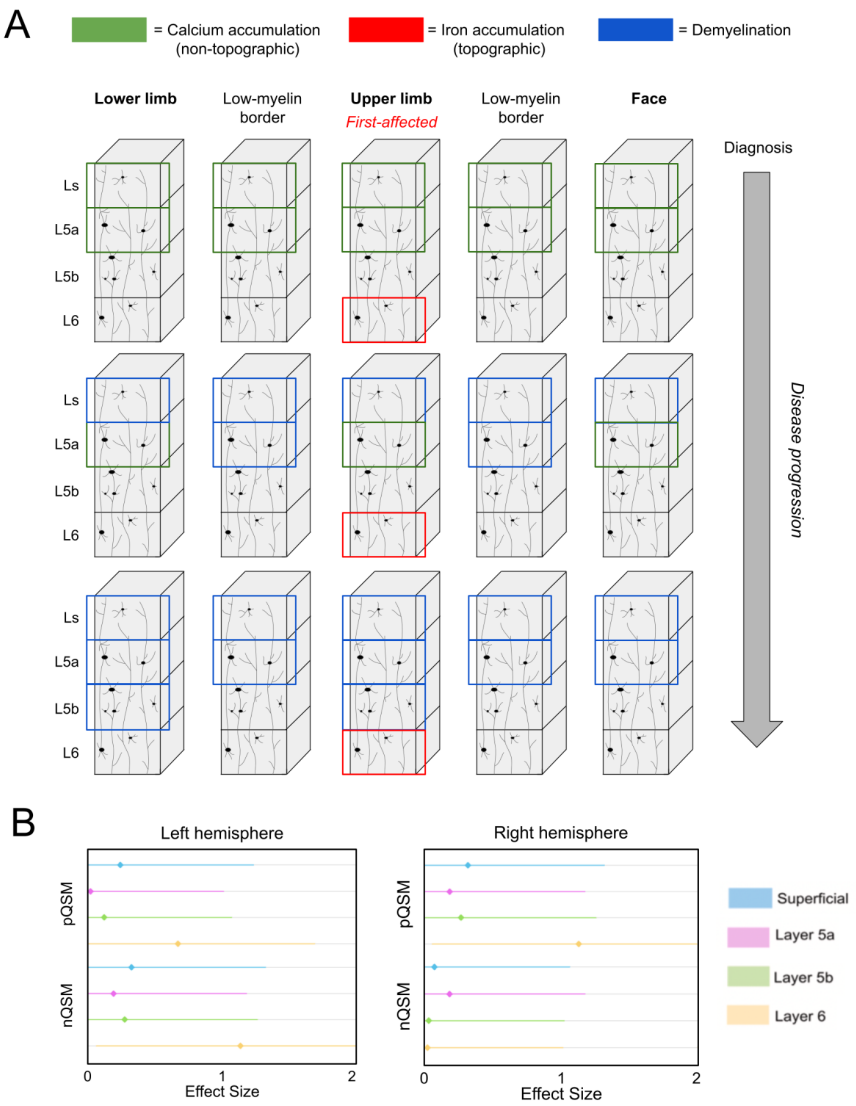


**Figure 4. Model of *in-vivo* disease mechanisms in ALS. (A)** Schematic depiction of the layer-specific pathology features shown in the ALS patients of the present study compared to matched controls. In the early disease stage, shortly after diagnosis, we demonstrate topographic (i.e. most in first-affected cortical field) iron accumulation in L6 and non-topographic (i.e. more widespread) calcium accumulation in Ls and L5a. With disease progression, we highlight increasing demyelination particularly in Ls and L5a, and in the low-myelin borders between adjacent cortical fields, corresponding to calcium accumulation at earlier time points. **(B)** Effect sizes of the layer-specific iron and calcium accumulation effects in ALS patients compared to matched controls (seeTable 3 for statistics). (L6 - layer 6, L5b - layer 5b, L5a - layer 5a, Ls - superficial layer).

Across cortical depth in M1, we show no significant differences in microstructure between patients and controls. Layer-specific analyses, however, reveal that iron accumulation in ALS is specific to L6 of M1. This extends previous studies showing deep iron accumulation in ALS, which may reflect neuroinflammation and activated microglia[6,15]. Our findings therefore suggest that iron accumulation in L6 may provide an earlier marker of pathology than the degeneration of L5(b)[5]. However, since the hotspots of iron accumulation largely matched the behaviorally affected body parts but often did not overlap with subsequent

demyelination, iron accumulation may be a consequence of disease progression rather than the cause.

Multimodal *in-vivo* pathology maps highlight iron accumulation in the first-affected cortical field as expected[17-19]. However, surface mapping reveals multiple, small hotspots of pathology rather than one large hotspot. For example, one patient (P1) shows L6 iron accumulation in an area between the LL and UL fields, which may reflect pathology in the torso region where impairment is difficult to detect. Another patient (P2) showed iron accumulation in Ls-L5a of the first-affected (UL) field, deviating from the expected location in L6, but in all layers of the contralateral F field. This may reflect the impaired tongue function in this patient, highlighting challenges in detecting bulbar-onset symptoms clinically[50]. Our findings demonstrate the mismatch between brain and behaviour in ALS[53] and emphasise the utility of MRI for individualised medicine.

We also investigated calcium dysregulation, demonstrating that Ls (including L2-L3) and L5a show calcium accumulation in ALS. Interestingly, this is not specific to the first-affected cortical fields and is therefore non-topographic. Instead, calcium is often increased in areas between cortical fields, where the low-myelin borders are located. Previous evidence has shown disrupted calcium homeostasis in ALS[7], where increased intracellular calcium is associated with glutamate excitotoxicity in animal models[20-21]. Increased calcium in humans may reflect similar mechanisms, including the increased activity of M1 in ALS[51] and/or calcifications in blood vessels related to poor brain health[52]. Interestingly, patients with pronounced calcium accumulation (P8, P12) largely show more focal behavioural impairment. This suggests that calcium accumulation provides an early disease marker which may be related to compensation, as suggested for increased activity[51].

While the early-affected patients were characterized by increased iron and calcium but preserved myelination, longitudinal data show widespread demyelination of M1 with disease progression. Critically, our data indicate that non-topographic calcium, rather than topographic iron accumulation, precedes demyelination. This is in line with evidence that metabolism changes and inflammation precede cell loss in ALS[54]. Demyelination largely affects Ls and L5a, reflecting the layer-specific calcium accumulation described above, and also particularly affects the low-myelin borders. These findings therefore do not support the

notion that L5(b) is first affected in ALS[5]. Rather, our data indicate that the low-myelin borders, that are connected to multiple body parts[23,26], play a role in disease spread.

An alternative perspective to this interpretation is that connections between low-myelin borders and subcortical structures[26] are more affected by pathology, compared to connections between cortical fields and subcortical structures. From this perspective, the affected border areas would not reflect markers of disease spread, but would be the consequence of affected subcortical systems. Further investigation is needed to characterize the role of non-topographic disease mechanisms in ALS. Although we used a method to define individual layers in M1 *in-vivo* based on an *in-vivo-ex-vivo* validation model[9-10], we can not guarantee that our layer definitions correspond to the exact biological layers. This limitation should be addressed with more extensive *in-vivo-ex-vivo* validation studies. Finally, although quantitative and validated markers of cortical microstructure were used here, we cannot be certain of the tissue properties measured.

In summary, we characterize *in-vivo* pathology in ALS-patients using topographic layer imaging. We provide novel evidence that non-topographic calcium accumulation may provide an early marker of disease spread in ALS[24]. Our study also highlights preserved layer architecture in M1, in addition to layer-specific iron accumulation, in ALS pathology. Finally, we show that the disruption of low-myelin borders may provide a novel mechanism of topographic disease spread. Our efficient 7T-MRI scanning protocol, and use of open-source analysis tools[35], make our approach highly accessible.

## Acknowledgements

The authors would like to thank the volunteer patients, and their families, for their participation in the study.

## Author Contributions

E.K. and S.S. designed the study. S.S, S.P. and J.P. recruited the patients. A.N., M.W. and J.D. collected the data. S.V. performed the clinical assessments. J.D., A.N. and I.T. developed the processing pipelines. A.N. completed the formal analysis, data investigation and statistical analysis. A.N. wrote the manuscript. E.K., J.D., S.S. and M.W. reviewed and edited the manuscript. E.K. and S.S. supervised the study. All authors contributed to the article and approved the submitted version.

## Funding

This project was funded by the Else Kröner Fresenius Stiftung: 2019-A03 and the Deutsche Forschungsgemeinschaft (DFG): KU 3711/2-1 (project number 423633679), SCHR 1418/5-1 (501214112) and Project-ID 425899996 – SFB 1436.

## Competing interests

The authors report no competing interests.

## References

1. Al-Chalabi A, Hardiman O, Kiernan MC, Chiò A, Rix-Brooks B, van den Berg LH. (2016). Amyotrophic lateral sclerosis: moving towards a new classification system. *The Lancet Neurology*. 2016;15(11),1182-1194.

2. Norris, F., Shepherd, R., Denys, E., Kwei, U., Mukai, E., Elias, L., ... & Norris, H. (1993). Onset, natural history and outcome in idiopathic adult motor neuron disease. *Journal of the neurological sciences*, *118*(1), 48-55.
3. Ravits JM, La Spada AR. ALS motor phenotype heterogeneity, focality, and spread: deconstructing motor neuron degeneration. *Neurology*. 2009;73(10),805-811.
4. Chio A, Logroscino G, Hardiman O, *et al*. Prognostic factors in ALS: a critical review. *Amyotrophic lateral sclerosis*. 2009;10(5-6),310-323.
5. Hammer RP, Tomiyasu U, Scheibel AB. Degeneration of the human Betz cell due to amyotrophic lateral sclerosis. *Experimental neurology*. 1979;63(2),336-346.
6. Kwan JY, Jeong SY, Van Gelderen P, *et al*. Iron accumulation in deep cortical layers accounts for MRI signal abnormalities in ALS: correlating 7 tesla MRI and pathology. *PloS one*. 2012;7(4),e35241.
7. Appel SH, Beers D, Siklos L, Engelhardt JI, Mosier DR. Calcium: the darth vader of ALS. *Amyotrophic Lateral Sclerosis and Other Motor Neuron Disorders*. 2001;2(1),47-54.
8. Sekiguchi T, Kanouchi T, Shibuya K, *et al*. Spreading of amyotrophic lateral sclerosis lesions—multifocal hits and local propagation?. *Journal of Neurology, Neurosurgery & Psychiatry*. 2014;85(1),85-91.
9. Huber L, Handwerker DA, Jangraw DC, *et al*. High-resolution CBV-fMRI allows mapping of laminar activity and connectivity of cortical input and output in human M1. *Neuron*. 2017;96(6),1253-1263.
10. Northall A, Doehler J, Weber M, Vielhaber S, Schreiber S, Kuehn E. Layer-specific vulnerability is a mechanism of topographic map aging. *Neurobiology of Aging*. 2023;128,17-32.
11. Doehler J, Northall A, Liu P, Fracasso A, Chrysidou A, Speck O, Lohmann G, Wolbers T, Kuehn E. The 3D Structural Architecture of the Human Hand Area Is Nontopographic. *Journal of Neuroscience*. 2023;43(19),3456-3476.
12. Acosta-Cabronero J, Machts J, Schreiber S, *et al*. Quantitative susceptibility MRI to detect brain iron in amyotrophic lateral sclerosis. *Radiology*. 2018a;289(1),195-203.
13. Adachi Y, Sato N, Saito Y, *et al*. Usefulness of SWI for the detection of iron in the motor cortex in amyotrophic lateral sclerosis. Journal of Neuroimaging. 2015;25(3),443-451.

14. Wang C, Foxley S, Ansorge O, *et al*. Methods for quantitative susceptibility and R2* mapping in whole post-mortem brains at 7T applied to amyotrophic lateral sclerosis. NeuroImage. 2020;222,117216.
15. Pallebage-Gamarallage M, Foxley S, Menke RA, *et al*. Dissecting the pathobiology of altered MRI signal in amyotrophic lateral sclerosis: A post mortem whole brain sampling strategy for the integration of ultra-high-field MRI and quantitative neuropathology. *BMC neuroscience*. 2018;19(1),1-24.
16. Cosottini M, Donatelli G, Costagli M, *et al*. High-resolution 7T MR imaging of the motor cortex in amyotrophic lateral sclerosis. *American journal of neuroradiology*. 2016;37(3),455-461.
17. Costagli M, Donatelli G, Biagi L, *et al*. Magnetic susceptibility in the deep layers of the primary motor cortex in amyotrophic lateral sclerosis. *NeuroImage: Clinical*. 2016;12,965-969.
18. Donatelli G, Ienco EC, Costagli M, *et al*. MRI cortical feature of bulbar impairment in patients with amyotrophic lateral sclerosis. *NeuroImage: Clinical*. 2019;24,101934.
19. Donatelli G, Costagli M, Cecchi P, *et al*. Motor cortical patterns of upper motor neuron pathology in amyotrophic lateral sclerosis: A 3 T MRI study with iron-sensitive sequences. *NeuroImage: Clinical*. 2022;35,103138.
20. Kruman II, Pedersen WA, Springer JE, Mattson MP. ALS-linked Cu/Zn–SOD mutation increases vulnerability of motor neurons to excitotoxicity by a mechanism involving increased oxidative stress and perturbed calcium homeostasis. *Experimental neurology*. 1999;160(1),28-39.
21. Siklós L, Engelhardt J, Harati Y, Smith RG., Joó F, Appel SH. Ultrastructural evidence for altered calcium in motor nerve terminals in amyotrophic lateral sclerosis. *Annals of neurology*. 1996;39(2),203-216.
22. Eisen A, Pant B, Stewart H. Cortical excitability in amyotrophic lateral sclerosis: a clue to pathogenesis. *Canadian journal of neurological sciences*. 1993;20(1),11-16.
23. Kuehn E, Dinse J, Jakobsen E, *et al*. Body topography parcellates human sensory and motor cortex. *Cerebral Cortex*. 2017;27(7),3790-3805.
24. Schreiber S, Northall A, Weber M, Vielhaber S, Kuehn E. Topographical layer imaging as a tool to track neurodegenerative disease spread in M1. *Nature Reviews Neuroscience*. 2021;22(1),68-69.

25. Bartzokis G, Lu PH, Mintz J. Human brain myelination and amyloid beta deposition in Alzheimer's disease. *Alzheimer's & dementia*. 2007;3(2),122-125.
26. Gordon EM, Chauvin RJ, Van AN, *et al*. A somato-cognitive action network alternates with effector regions in motor cortex. *Nature*. 2023;1-9.
27. Stüber C, Morawski M, Schäfer A, *et al*. Myelin and iron concentration in the human brain: a quantitative study of MRI contrast. *Neuroimage*. 2014;93,95-106.
28. Wang Y, Spincemaille P, Liu Z, *et al*. Clinical quantitative susceptibility mapping (QSM): Biometal imaging and its emerging roles in patient care. *Journal of magnetic resonance imaging*. 2017;46(4),951-971.
29. Brooks BR, Miller RG, Swash M, Munsat TL. El Escorial revisited: revised criteria for the diagnosis of amyotrophic lateral sclerosis. *Amyotrophic lateral sclerosis and other motor neuron disorders*. 2000;1(5),293-299.
30. Cedarbaum JM, Stambler N, Malta E, *et al*. The ALSFRS-R: a revised ALS functional rating scale that incorporates assessments of respiratory function. *Journal of the neurological sciences*. 1999;169(1-2),13-21.
31. Moore SR, Gresham LS, Bromberg MB, Kasarkis EJ, Smith RA. A self report measure of affective lability. *Journal of Neurology, Neurosurgery & Psychiatry*. 1997;63(1),89-93.
32. Smith RA, Macklin EA, Myers KJ, *et al*. Assessment of bulbar function in amyotrophic lateral sclerosis: validation of a self‐report scale (Center for Neurologic Study Bulbar Function Scale). *European journal of neurology*. 2018;25(7),907-e66.
33. Quinn C, Edmundson C, Dahodwala N, Elman L. Reliable and efficient scale to assess upper motor neuron disease burden in amyotrophic lateral sclerosis. *Muscle & nerve*. 2020;61(4),508-511.
34. Marques JP, Kober T, Krueger, G, van der Zwaag W, Van de Moortele PF, Gruetter R. MP2RAGE, a self bias-field corrected sequence for improved segmentation and T1-mapping at high field. *Neuroimage*. 2010;49(2),1271-1281.
35. Bazin PL, Weiss M, Dinse J, Schäfer A, Trampel R, Turner R. A computational framework for ultra-high resolution cortical segmentation at 7 Tesla. *NeuroImage*. 2014;93,201-209.
36. McAuliffe MJ, Lalonde FM, McGarry D, Gandler W, Csaky K, Trus BL. Medical image processing, analysis and visualization in clinical research. *In Proceedings 14th IEEE Symposium on Computer-Based Medical Systems*. 2001,381-386.

37. Bazin PL, Pham DL. Homeomorphic brain image segmentation with topological and statistical atlases. *Medical image analysis*. 2008;12(5),616-625.
38. Han X, Pham DL, Tosun D, Rettmann ME, Xu C, Prince JL. CRUISE: cortical reconstruction using implicit surface evolution. *NeuroImage*. 2004;23(3),997-1012.
39. Waehnert MD, Dinse J, Weiss M, *et al*. Anatomically motivated modeling of cortical laminae. *Neuroimage*. 2014;93,210-220.
40. Waehnert MD, Dinse J, Schäfer A, *et al*. A subject-specific framework for in vivo myeloarchitectonic analysis using high resolution quantitative MRI. *Neuroimage*. 2016;125,94-107.
41. Acosta-Cabronero J, Milovic C, Mattern H, Tejos C, Speck O, Callaghan MF. A robust multi-scale approach to quantitative susceptibility mapping. *Neuroimage*. 2018b;183,7-24.
42. Betts MJ, Acosta-Cabronero J, Cardenas-Blanco A, Nestor PJ, Düzel E. High-resolution characterisation of the aging brain using simultaneous quantitative susceptibility mapping (QSM) and R2* measurements at 7 T. *Neuroimage*. 2016;138,43-63.
43. Sereno MI, Lutti A, Weiskopf N, Dick F. Mapping the human cortical surface by combining quantitative T 1 with retinotopy. *Cerebral cortex*. 2013;23(9),2261-2268.
44. Glasser MF, Coalson TS, Robinson EC, *et al*. A multi-modal parcellation of human cerebral cortex. *Nature*. 2016;536(7615),171-178.
45. Enright PL. The six-minute walk test. *Respiratory care*. 2003;48(8),783-785.
46. Peolsson A, Hedlund R, Öberg B. Intra-and inter-tester reliability and reference values for hand strength. *Journal of rehabilitation medicine*. 2001;33(1),36-41.
47. Tiffin J, Asher EJ. The Purdue Pegboard: norms and studies of reliability and validity. *Journal of applied psychology*. 1948;32(3),234.
48. Matthews, C. G., & Klove, H. (1964). Instruction manual for the adult neuropsychology test battery. Madison, WI: University of Wisconsin Medical School, 36.
49. Fleishman EA. A modified administration procedure for the O'Connor Finger Dexterity Test. *Journal of Applied Psychology*. 1953;37(3),191.
50. Northall, A., Mukhopadhyay, B., Weber, M., Petri, S., Prudlo, J., Vielhaber, S., ... & Kuehn, E. (2022). An automated tongue tracker for quantifying bulbar function in ALS. *Frontiers in Neurology*, 223.

51. Proudfoot M, Bede P, Turner MR. Imaging cerebral activity in amyotrophic lateral sclerosis. *Frontiers in neurology*. 2019;9,1148.
52. Schreiber S, Bernal J, Arndt P, *et al*. Brain vascular health in ALS is mediated through motor cortex microvascular integrity. *Cells*. 2023;12(6),957.
53. Verstraete E, Turner MR, Grosskreutz J, *et al*. Mind the gap: the mismatch between clinical and imaging metrics in ALS. *Amyotrophic lateral sclerosis and frontotemporal degeneration*. 2015;16(7-8),524-529.
54. Toft MH, Gredal O, Pakkenberg B. The size distribution of neurons in the motor cortex in amyotrophic lateral sclerosis. *Journal of anatomy*. 2005;207(4),399-407.
55. Maranzano A, Verde F, Colombo E, Poletti B, Doretti A, Bonetti R, Gagliardi D, Meneri M, Corti S, Morelli C, Silani V & Ticozzi N. Regional spreading pattern is associated with clinical phenotype in amyotrophic lateral sclerosis. *Brain*. 2023; doi: 10.1093/brain/awad129.
56. Dinse J, Härtwich N, Waehnert MD, *et al*. A cytoarchitecture-driven myelin model reveals area-specific signatures in human primary and secondary areas using ultra-high resolution in-vivo brain MRI. *Neuroimage*. 2015;114,71-87.
57. Vogt C, Vogt O. Allgemeine Ergebnisse unserer Hirnforschung [General results of our brain research]. *Zeitschrift für Augenheilkunde*. 1919;25,273–462.